EVALUATION OF INSTABILITY FORCES OF LABYRINTH SEALS IN TURBINES OR COMPRESSORS

Takuzo Iwatsubo
Faculty of Engineering, Kobe University,
Rokko, Nada, Kobe, 657 Japan

SUMMARY

This work investigates the effects of a force induced by the labyrinth seal on the stability of rotor systems and the factors of the seal which affect the stability. In the analysis, it is assumed that the fluid in the seal is steady and that the rotor is set vertically in order to avoid the effects of gravity force. The force induced by the seal is expressed in terms proportional to the velocity and displacement of the rotor and is deduced to that expression for the oil-film force in journal bearings. That force is taken into account in the equations of motion; then the stability of the system is discussed by energy concept.

The force induced by the labyrinth seal always makes the rotor system unstable, and the tendency is remarkable when seal leakages are small. The resonance point of the rotor system is also affected by the labyrinth seal; that is, the resonance point of the rotor system is removed by the seal leakages. The flow pattern in the labyrinth seal was investigated experimentally, and the force induced by the labyrinth seal was measured by using a water-tunnel experimental system which was designed to measure the labyrinth seal force by using the similarity between gas and liquid flow theory.

INTRODUCTION

After the oil shock, high-performance turbines and compressors are required in order to save energy. For this purpose, designers would like to minimize leakage from labyrinth seals, so they design the clearances of the labyrinth seal to be small. However, if the clearances are small, self-excited rotor vibrations are caused by the flow forces of the working fluid. The origins of the exciting forces are at present only partially known as a steam whirl excitation. So it is not enough to evaluate these forces in order to design the labyrinth seals for compressors and turbines. Thus the analysis of labyrinth seals and the materials for design are strongly required by the designer of turbines and compressors. This paper is devoted to a basic analysis of the fluid force due to labyrinth seals.

First, the fundamental equation proposed by Kostyuk (refs. 1,2) is extended in order to consider the effect of the variation of gland cross section. For the analysis, the fundamental equation is rewritten to ordinary differential equations by using the finite difference method. Then spring and damping coefficients of the labyrinth seals are calculated for selected models from the fundamental equation and perturbation from the steady state. The flow rate and pressure, etc., in the steady state are also calculated. Then the stability of

the rotor system is discussed in terms of these coefficients by using the concept of energy. Furthermore, experiments were executed to observe the flow pattern in the gland and to study the characteristics of the flow-induced forces in the labyrinth seals.

FUNDAMENTAL EQUATION FOR GAS FLOW IN LABYRINTH SEAL

For the derivation of the equations, the following conditions are assumed;

(1) Fluid in the labyrinth seal is assumed to be gas, and its behavior is assumed to be ideal.

(2) Temperature of the fluid in the labyrinth seal is assumed to be constant.

(3) Cross-sectional area of the seal gland is assumed to be constant in spite of the deflection of rotor, and only the time derivative of the cross-sectional area is considered.

(4) Change of flow state in the gland is assumed to be isentropic.

Thus from the illustrations of figure 1 the fundamental equations with respect to the flow rate and pressure are as follows;

$$\frac{\partial(\rho_i f_i)}{\partial t} + f_i \frac{\partial(\rho_i C_i)}{\partial w} + (g_{i+1} - g_i) = 0 \tag{1}$$

$$f_i \frac{\partial(\rho_i C_i^2)}{\partial w} + \frac{\partial(\rho_i f_i C_i)}{\partial t} + (g_{i+1} C_i - g_i C_{i-1}) + \tau' U' - \tau'' U'' = -f_i \frac{\partial p_i}{\partial w} \tag{2}$$

$$\tau' = \frac{1}{2} \lambda' \rho_i C_i^2 \tag{3}$$

$$\tau'' = \frac{1}{2} \lambda'' \rho_i (u - C_i)^2 \tag{4}$$

$$p_{i-1}^2 - p_i^2 = \frac{g_i^2 RT}{\mu_i^2 \delta_i^2} \tag{5}$$

$$p_i = \rho_i g RT \tag{6}$$

$$Re = \frac{C\varepsilon}{\nu} \tag{7}$$

Equations (1) to (7) are nonlinear partial differential equations; so for the analysis they must be rewritten to linear partial differential equations by using the perturbation terms from the steady state. Therefore, pressure, axial flow rate, and peripheral velocity in the steady state should be obtained.

ANALYSIS OF FLOW IN STEADY STATE

As the flow in the seal is steady, all state variables are constant; therefore time derivatives and space derivatives of the state variables are zero. Thus the fundamental equations become as follows:

$$q_{i+1} - q_i = 0 \tag{8}$$

$$q_{i+1} C_i - q_i C_{i-1} + \tau' U' - \tau'' U'' = 0 \tag{9}$$

From these equations, state variables in the equilibrium condition are obtained by using the iterative method as shown in figure 2. For this calculation, the pressure recovery factor η_p is

$$\eta_p = \frac{2A}{1+A}$$

where

$$A = \frac{(\delta/l) C_c}{(\delta/l) + \tan\Theta} \tag{10}$$

and Θ is the angle between the rotating axis and the flow direction passing through the seal strip.

The steady-state flow rate is given as

$$q_{*i} = \alpha_i \delta_{*i} g \sqrt{\frac{2\kappa}{\kappa-1} \cdot p'_{*i-1} \cdot \rho'_{*i-1} \left[\left(\frac{p_{*i}}{p'_{*i-1}} \right)^{2/\kappa} - \left(\frac{p_{*i}}{p'_{*i-1}} \right)^{\kappa+1/\kappa} \right]} \tag{11}$$

LINEARIZATION OF FUNDAMENTAL EQUATION

For the linearization of the fundamental equation, the perturbations of pressure, peripheral velocity, and flow rate from those of the steady state are introduced as

$$p_i = p_{*i}(1 + \xi_i) \tag{12}$$

$$C_i = C_{*i}(1 + \eta_i) \tag{13}$$

$$q_i = q_{*i}(1 + \zeta_i) \tag{14}$$

where P_{*i}, C_{*i}, and q_{*i} are pressure, peripheral velocity, and axial flow rate of steady state in the i^{th} gland and ξ_i, η_i, and ζ_i are the nondimensional perturbation terms of pressure, peripheral velocity, and axial flow rate.

The cross-sectional area in the i^{th} gland is represented as

$$f_i = l(h_i + \delta_i) \tag{15}$$

where h_i and δ_i are the height of the gland and the radial labyrinth clearance.

By denoting the displacement of the center of the rotor (x,y) as

$$\begin{aligned} x &= r_1 \cos \Omega t \\ y &= r_2 \sin \Omega t \end{aligned} \tag{16}$$

the area of the i^{th} chamber section is obtained as

$$f_i = l(h_i + \delta_{*i} - \delta_{*i} r_1 \cos \Omega t \cos \varphi - \delta_{*i} r_2 \sin \Omega t \sin \varphi) \tag{17}$$

Because the change of state in the gland is isentropic change, the following relation is obtained:

$$\frac{P_{*i}}{\rho_{*i}^{\varkappa}} = \frac{P_i}{\rho_i^{\varkappa}} = const$$

Therefore

$$\frac{\partial P_i}{\partial t} = \varkappa \frac{P_i}{\rho_i} \frac{\partial \rho_i}{\partial t} \tag{18}$$

From the above equations, the following linear equations are obtained:

$$\frac{l}{\kappa}(h_i+\delta_{*i})\dot{\xi}_i+\frac{C_{*i}l}{\kappa R_s}(h_i+\delta_{*i})\xi_i'+\frac{C_{*i}l}{R_s}(h_i+\delta_{*i})\eta_i'$$
$$-\frac{gRT\mu^2\delta_{*i+1}^2P_{*i+1}^2}{P_{*i}g_*}\xi_{i+1}+\frac{gRT\mu^2P_{*i}}{g_*}(\delta_{*i+1}^2+\delta_{*i}^2)\xi_i$$
$$-\frac{gRT\mu^2\delta_{*i}^2P_{*i-1}^2}{P_{*i}g_*}\xi_{i-1}+\frac{gRT\mu^2\delta_{*i+1}^2}{2P_{*i}g_*}(P_{*i}^2-P_{*i+1}^2)$$
$$-\frac{gRT\mu^2\delta_{*i}^2}{2P_{*i}g_*}(P_{*i-1}^2-P_{*i}^2)=\frac{gRT\mu^2}{P_{*i}g_*}\{\delta_{*i+1}(P_{*i}^2-P_{*i+1}^2)$$
$$+\delta_{*i}(P_{*i}^2-P_{*i-1}^2)\}(r_1\cos\Omega t\cos\varphi+r_2\sin\Omega t\sin\varphi)$$
$$+l(-r_1\Omega\sin\Omega t\cos\varphi+r_2\Omega\cos\Omega t\sin\varphi) \qquad (19)$$

$$\frac{l}{\kappa}(h_i+\delta_{*i})\dot{\xi}_i+l(h_i+\delta_{*i})\dot{\eta}_i+\frac{l(h_i+\delta_{*i})}{R_s}\left(\frac{C_*}{\kappa}+\frac{gRT}{C_*}\right)\xi_i'$$
$$+\frac{2C_*l}{R_s}(h_i+\delta_{*i})\eta_i'-\frac{gRT\mu^2\delta_{*i+1}^2P_{*i+1}^2}{P_{*i}g_*}\xi_{i+1}+\left(\frac{\lambda'U_i'C_*}{2}+\frac{gRT\mu^2\delta_{*i+1}^2P_{*i}}{g_*}\right.$$
$$\left.+\frac{gRT\mu^2\delta_{*i}^2P_{*i}}{g_*}-\frac{\lambda''U_i''(u-C_*)^2}{2C_*}\right)\xi_i-\frac{gRT\mu^2\delta_{*i}^2P_{*i-1}^2}{P_{*i}g_*}\xi_{i-1}$$
$$+\left(\lambda'U_i'C_*-\lambda''U_i''(C_*-u)+\frac{gRTg_*}{P_{*i}}\right)\eta_i-\frac{gRTg_*}{P_{*i}}\eta_{i-1}$$
$$+\frac{\lambda'U_i'C_*}{2}-\frac{\lambda''U_i''(u-C_*)^2}{2C_*}+\frac{gRT\mu^2}{2g_*}\left(\delta_{*i+1}^2P_{*i}-\delta_{*i+1}^2\frac{P_{*i+1}^2}{P_{*i}}-\delta_{*i}^2\frac{P_{*i-1}^2}{P_{*i}}\right.$$
$$\left.+\delta_{*i}^2P_{*i}\right)=\frac{gRT\mu^2}{g_*}\left(\delta_{*i+1}P_{*i}-\delta_{*i+1}\frac{P_{*i+1}^2}{P_{*i}}-\delta_{*i}\frac{P_{*i-1}^2}{P_{*i}}+\delta_{*i}P_{*i}\right)$$
$$\times(r_1\cos\Omega t\cos\varphi+r_2\sin\Omega t\sin\varphi)$$
$$+l(-r_1\Omega\sin\Omega t\cos\varphi+r_2\Omega\cos\Omega t\sin\varphi) \qquad (20)$$

where

$$(\dot{\cdot}) = \frac{\partial(\cdot)}{\partial t} \quad , \quad (\cdot)' = \frac{\partial(\cdot)}{\partial \varphi}$$

Equations (19) and (20) are rewritten in the matrix form as

$$\mathbb{T}\dot{\mathbb{U}} + \mathbb{V}\mathbb{U}' + \mathbb{B}\mathbb{U} = \mathbb{f}\left(r_1 \cos\Omega t \cos\varphi + r_2 \sin\Omega t \sin\varphi\right) + \mathbb{g}\left(r_1 \sin\Omega t \cos\varphi - r_2 \cos\Omega t \sin\varphi\right) \qquad (21)$$

where T, V, and B are (2k - 1) × (2k - 1) matrix and u, f and g are (2k - 1) row vectors and u is represented as

$$\mathbb{U}^T = \lfloor \xi_1, \eta_1, \xi_2, \eta_2, \cdots, \xi_{k-1}, \eta_{k-1}, 1 \rfloor$$

ANALYSIS BY FINITE DIFFERENCE METHOD

Multiplying equation (21) by T^{-1} yields

$$\mathbb{I}\dot{\mathbb{U}} + \mathbb{D}\mathbb{U}' + \mathbb{Q}\mathbb{U} = \mathbb{S}\left(r_1 \cos\Omega t \cos\varphi + r_2 \sin\Omega t \sin\varphi\right) + \mathbb{r}\left(r_1 \sin\Omega t \cos\varphi - r_2 \cos\Omega t \sin\varphi\right) \qquad (22)$$

where

$$\mathbb{D} = \mathbb{T}^{-1}\mathbb{V} \quad , \quad \mathbb{Q} = \mathbb{T}^{-1}\mathbb{B}$$
$$\mathbb{S} = \mathbb{T}^{-1}\mathbb{f} \quad , \quad \mathbb{r} = \mathbb{T}^{-1}\mathbb{g}$$
$$\mathbb{I} = \text{unit matrix}$$

By dividing the circumferential space of the rotor into n elements as shown in figure 3, the following finite difference equation is obtained about the j^{th} element:

$$\mathbb{I}\dot{\mathbb{U}}_j + \mathbb{P}(\mathbb{U}_{j+1} - \mathbb{U}_{j-1}) + \mathbb{Q}\mathbb{U}_j = \mathbb{a}_j \cos\Omega t + \mathbb{b}_j \sin\Omega t + \mathbb{c}_j \sin\Omega t - \mathbb{d}_j \cos\Omega t \qquad (23)$$

where

$$\mathbb{P} = \mathbb{D}/2\Delta\,,\quad \mathfrak{a}_j = \$\, r_1 \cos\varphi_j\,,\quad \mathfrak{b}_j = \$\, r_2 \sin\varphi_j$$

$$\mathbb{C}_j = \mathbb{r}\, r_1 \cos\varphi_j\,,\quad \mathfrak{d}_j = \mathbb{r}\, r_2 \sin\varphi_j\,,$$

$$\mathbb{U}_j^T = \lfloor\, u_{1j}, u_{2j}, \text{-----}, u_{ij}, \text{----}, u_{k-1\,j}, 1 \,\rfloor$$

$$\mathfrak{a}_j^T = \lfloor\, a_{1j}, a_{2j}, \text{-----}, a_{ij}, \text{-----}, a_{k-1\,j}, 0 \,\rfloor$$

$$\mathfrak{b}_j^T = \lfloor\, b_{1j}, b_{2j}, \text{-----}, b_{ij}, \text{-----}, b_{k-1\,j}, 0 \,\rfloor$$

$$\mathfrak{C}_j^T = \lfloor\, c_{1j}, c_{2j}, \text{-----}, c_{ij}, \text{-----}, c_{k-1\,j}, 0 \,\rfloor$$

$$\mathfrak{d}_j^T = \lfloor\, d_{1j}, d_{2j}, \text{-----}, d_{ij}, \text{-----}, d_{k-1\,j}, 0 \,\rfloor$$

When the boundary conditions are set as $u_j(\phi_j, t) = u_j(\phi_j + 2\pi, t)$, equation (23) is reduced for the overall system to

$$\mathbb{I}\dot{\mathbb{X}} + \mathbb{A}\mathbb{X} = \mathfrak{a}\cos\Omega t + \mathfrak{b}\sin\Omega t + \mathfrak{C}\sin\Omega t - \mathfrak{d}\cos\Omega t \qquad (24)$$

where x, a, b, c, d are $n(2k-1)$ row vectors and A is $n(2k-1) \times n(2k-1)$ matrix

The solution of equation (24) is obtained in matrix form as

$$\mathbb{X} = e^{-\mathbb{A}t}\mathfrak{e} + \int_0^t e^{-(t-s)\mathbb{A}}\,\mathfrak{a}\cos\Omega s\,ds + \int_0^t e^{-(t-s)\mathbb{A}}\,\mathfrak{b}\sin\Omega s\,ds$$
$$+ \int_0^t e^{-(t-s)\mathbb{A}}\,\mathfrak{C}\sin\Omega s\,ds - \int_0^t e^{-(t-s)\mathbb{A}}\,\mathfrak{d}\cos\Omega s\,ds \qquad (25)$$

If the rotor is rotating at the steady state, the perturbation terms are equal to zero; so the initial condition for analysis becomes

$$\mathfrak{e} = 0 \qquad (26)$$

By using this condition, equation (25) becomes

$$\mathbb{X} = \mathbb{E}\, r_1 \cos\Omega t + \mathbb{F}\, r_2 \sin\Omega t + \mathbb{G}(-r_1\Omega \sin\Omega t)$$
$$+ \mathbb{H}\, r_2\Omega \cos\Omega t \qquad (27)$$

where

$$\mathbb{E} = \frac{1}{r_1}\left\{\frac{1}{\Omega^2}\left(\mathbb{I} + \frac{\mathbb{A}^2}{\Omega^2}\right)^{-1}\mathbb{A}\,\mathbb{a} - \frac{1}{\Omega}\left(\mathbb{I} + \frac{\mathbb{A}^2}{\Omega^2}\right)^{-1}\mathbb{b}\right\}$$

$$\mathbb{F} = \frac{1}{r_2}\left\{\frac{1}{\Omega^2}\left(\mathbb{I} + \frac{\mathbb{A}^2}{\Omega^2}\right)^{-1}\mathbb{A}\,\mathbb{b} + \frac{1}{\Omega}\left(\mathbb{I} + \frac{\mathbb{A}^2}{\Omega^2}\right)^{-1}\mathbb{a}\right\}$$

$$\mathbb{G} = \frac{1}{r_1\Omega}\left\{\frac{1}{\Omega}\left(\mathbb{I} + \frac{\mathbb{A}^2}{\Omega^2}\right)^{-1}\mathbb{d} - \frac{1}{\Omega^2}\left(\mathbb{I} + \frac{\mathbb{A}^2}{\Omega^2}\right)^{-1}\mathbb{A}\,\mathbb{C}\right\}$$

$$\mathbb{H} = \frac{1}{r_2\Omega}\left\{-\frac{1}{\Omega}\left(\mathbb{I} + \frac{\mathbb{A}^2}{\Omega^2}\right)^{-1}\mathbb{C} - \frac{1}{\Omega^2}\left(\mathbb{I} + \frac{\mathbb{A}^2}{\Omega^2}\right)^{-1}\mathbb{A}\,\mathbb{d}\right\}$$

By using the nondimensional variable of pressure, fluid forces acting on the rotor are given as

$$\begin{aligned} F_x &= -R_s \sum_{i=1}^{k-1} \int_0^{2\pi} P_{*i}\,\xi_i\,\ell\cos\varphi\,d\varphi \\ &\fallingdotseq -\frac{2\pi R_s \ell}{n}\sum_{i=1}^{k-1} P_{*i}\sum_{j=1}^{n}\xi_{ij}\cos\left(\frac{2\pi}{n}(j-1)\right) \end{aligned}$$

$$\begin{aligned} F_y &= -R_s \sum_{i=1}^{k-1} \int_0^{2\pi} P_{*i}\,\xi_i\,\ell\sin\varphi\,d\varphi \\ &\fallingdotseq -\frac{2\pi R_s \ell}{n}\sum_{i=1}^{k-1} P_{*i}\sum_{j=1}^{n}\xi_{ij}\sin\left(\frac{2\pi}{n}(j-1)\right) \end{aligned} \qquad (28)$$

where ξ_{ij} is nondimensional variable of the i^{th} gland and the j^{th} element. By applying the relation

$$\begin{aligned} r_1\cos\Omega t = x \quad , \quad r_2\sin\Omega t = y \\ -r_1\Omega\sin\Omega t = \dot{x} \quad , \quad r_2\Omega\cos\Omega t = \dot{y} \end{aligned} \qquad (29)$$

to equation (28), the flow-induced force due to the labyrinth seal is obtained as

$$\begin{aligned} F_x &= k_{xx}x + k_{xy}y + C_{xx}\dot{x} + C_{xy}\dot{y} \\ F_y &= k_{yx}x + k_{yy}y + C_{yx}\dot{x} + C_{yy}\dot{y} \end{aligned} \qquad (30)$$

where

$$k_{xx} = -\frac{2\pi R_s l}{n}\sum_{i=1}^{k-1} P_{*i}\sum_{j=1}^{n} \mathbb{E}_{\xi_{ij}} \cos\left(\frac{2\pi}{n}(j-1)\right)$$

$$k_{xy} = -\frac{2\pi R_s l}{n}\sum_{i=1}^{k-1} P_{*i}\sum_{j=1}^{n} \mathbb{F}_{\xi_{ij}} \cos\left(\frac{2\pi}{n}(j-1)\right) \qquad (31)$$

$$C_{xx} = -\frac{2\pi R_s l}{n}\sum_{i=1}^{k-1} P_{*i}\sum_{j=1}^{n} \mathbb{G}_{\xi_{ij}} \cos\left(\frac{2\pi}{n}(j-1)\right)$$

$$C_{xy} = -\frac{2\pi R_s l}{n}\sum_{i=1}^{k-1} P_{*i}\sum_{j=1}^{n} \mathbb{H}_{\xi_{ij}} \cos\left(\frac{2\pi}{n}(j-1)\right) \qquad (32)$$

$$k_{yx} = -\frac{2\pi R_s l}{n}\sum_{i=1}^{k-1} P_{*i}\sum_{j=1}^{n} \mathbb{E}_{\xi_{ij}} \sin\left(\frac{2\pi}{n}(j-1)\right)$$

$$k_{yy} = -\frac{2\pi R_s l}{n}\sum_{i=1}^{k-1} P_{*i}\sum_{j=1}^{n} \mathbb{F}_{\xi_{ij}} \sin\left(\frac{2\pi}{n}(j-1)\right) \qquad (33)$$

$$C_{yx} = -\frac{2\pi R_s l}{n}\sum_{i=1}^{k-1} P_{*i}\sum_{j=1}^{n} \mathbb{G}_{\xi_{ij}} \sin\left(\frac{2\pi}{n}(j-1)\right)$$

$$C_{yy} = -\frac{2\pi R_s l}{n}\sum_{i=1}^{k-1} P_{*i}\sum_{j=1}^{n} \mathbb{H}_{\xi_{ij}} \sin\left(\frac{2\pi}{n}(j-1)\right) \qquad (34)$$

These coefficients are the spring constants and damping coefficients for the gas flow through the labyrinth seal when the rotor moves parallel to the casing axis.

NUMERICAL EXAMPLE

The labyrinth seal having three teeth is used as a numerical model, and the seal is divided into 24 elements for the finite difference method. Details of the labyrinth seal, the rotor, and the fluid are shown in tables 1 to 3. In table 1, models A to C investigate the effect of seal clearance, models D to F investigate the effect of precession, and models G and H investigate the effect of divergence and convergence seals.

For the calculation, the following values are used:

Flow coefficient = 0.7

$\lambda = 64/Re$ for $Re < 1200$

$\lambda = 0.3164 Re^{-0.25}$ for $Re \geq 1200$

where Re is Reynolds number.

Table 4 shows the pressure and flow rate in the steady state. Figures 4 to 6 show the spring constants and damping coefficients for each model. Because the rotor axis is coincident with the casing axis for the calculation, the following relations are obtained:

$$\begin{aligned} Kxx &= Kyy, \qquad Kxy = -Kxy \\ Cxx &= Cyy, \qquad Cxy = -Cyx \end{aligned} \tag{35}$$

Figure 4 shows the spring constants and damping constants for models A, B, and C in order to investigate the effect of clearance. From figure 4(b), principal diagonal terms of the damping coefficients are constant for the variation of rotating speed; on the other hand, the cross terms of the damping coefficient vary with rotating speed. Decreasing the clearance makes the coefficients large. Figure 5 shows the effect of precession, from which it is known that the diagonal terms of both the spring and damping coefficients are constant for the variation of rotating speed but that the cross terms of both the spring and damping coefficients are strongly dependent on rotating speed. Figure 6 shows the different effects of convergence and divergence seals. From these figures it becomes clear that the cross terms of the spring coefficients and the damping coefficients are quantitatively different.

ENERGETIC APPROACH TO STABILITY

In this section, the energy, eigenvalue, and phase difference between two modes are derived for a two-degree-of-freedom system, and the result is applied to the stability analysis of a rotor having a labyrinth seal. The general equation of motion is represented in matrix form as

$$\mathbb{M}\ddot{\mathbb{X}} + \mathbb{B}\dot{\mathbb{X}} + \mathbb{K}\mathbb{X} = \mathbb{0} \tag{36}$$

where

$$\mathbb{X} = \begin{Bmatrix} x_1 \\ x_2 \end{Bmatrix}, \quad \mathbb{M} = \begin{bmatrix} m_{11} & 0 \\ 0 & m_{22} \end{bmatrix}, \quad \mathbb{B} = \begin{bmatrix} b_{11} & b_{12} \\ b_{21} & b_{22} \end{bmatrix}, \quad \mathbb{K} = \begin{bmatrix} k_{11} & k_{12} \\ k_{21} & k_{22} \end{bmatrix}$$

As equation (36) has two eigenvalues, we consider the energy for each mode by assuming the periodical vibrational mode, that is, by neglecting the real part of the eigenvalue. Then the vibrational energy for one cycle for each mode is written as

$$E = \int \dot{\mathbb{X}}^T \mathbb{M} \ddot{\mathbb{X}} dt + \int \dot{\mathbb{X}}^T \mathbb{B} \dot{\mathbb{X}} dt + \int \dot{\mathbb{X}}^T \mathbb{K} \mathbb{X} dt \tag{37}$$

The first term of expression (37) is kinetic energy, the second is dissipative energy, and the third is potential energy. The energies of each term for one cycle (one period = τ) are obtained as

$$\int_0^\tau \dot{x}^T M \ddot{x}\, dt = 0 \tag{38}$$

$$\int_0^\tau \dot{x}^T B \dot{x}\, dt = \int_0^\tau (b_{11}\dot{x}_1^2 + b_{22}\dot{x}_2^2 + 2\bar{b}\dot{x}_1\dot{x}_2)dt \equiv E_1 + E_2 \tag{39}$$

where

$$\bar{b} = \frac{1}{2}(b_{12} + b_{21})$$

$$\int_0^\tau \dot{x}^T K x\, dt = \int_0^\tau \Delta k(\dot{x}_1 x_2 - x_1 \dot{x}_2)dt \equiv E_3 \tag{40}$$

where

$$\Delta k = \frac{1}{2}(k_{12} - k_{21})$$

Therefore the total energy of the system for one cycle becomes

$$E = E_1 + E_2 + E_3 \quad , \tag{41}$$

where

$$E_1 = \frac{\omega_j}{\omega}(b_{11}u_1^2 + b_{22}u_2^2) \, ,$$

$$E_2 = \frac{\omega_j}{\omega} \cdot 2\bar{b}\, u_1 u_2 \cos(\phi_1 - \phi_2) \, , \tag{42}$$

$$E_3 = -2\Delta k\, u_1 u_2 \sin(\phi_1 - \phi_2) \, ,$$

u_i is the eigenvector and $(\phi_1 - \phi_2)$ is the phase angle between the first and second modes. By using this result, the stability of the system may be stated from the energy point of view as follows:

(1) If $E > 0$, the energy of the system is absorbed, and thus the system is stable.

(2) If $E < 0$, the energy of the system is dissipative, and thus the system is unstable.

In expression (42), E_i is the energy obtained by diagonal elements of the damping coefficient. It is always positive; so if the damping coefficient is positive, this term always makes the system stable. Also E_2 is the energy obtained by cross elements of the damping coefficient, and its sign is dependent on the phase angle between ϕ_1 and ϕ_2. Finally E_3 is the energy obtained by cross elements of $(k_{12} - k_{21})$ and the phase angle between ϕ_1 and ϕ_2.

From the above discussion, cross elements of the stiffness and the diagonal elements of the damping make the system unstable, and the cross elements of the damping do not affect the stability in this case.

EXPERIMENTS

The experimental apparatus shown in figure 7 was used to observe the flow pattern in the labyrinth seal and to investigate the dynamic behavior of the labyrinth seal. The rotor is driven by a variable-speed motor system, and its bearing (with eccentricity) is also driven by another variable-speed motor in order to obtain an arbitrary whirling speed and spinning speed. A two-stage labyrinth seal (straight type) is set up at the rotor, whose depth of gland, pitch, and mean clearance are 18.2, 30.0, and 1.8 millimeters, respectively. Rotating speed of the rotor and shaft for whirling drive are 84 337 and 93 460 rpm, respectively. The casing is made from polymethyl-meta-acrylate in order to show the flow state, and water is used for the working fluid.

Pressure in the shroud is measured by the semiconductor pressure gage, and its signal is analyzed by a real-time analyzer. Figure 8 shows the flow pattern in the shroud, where a continuous vortex in the circumferential direction occurs in the fluid flow. The form is like a sinusoidal wave which is rotating in the same direction as the rotor. Figures 9 and 10 show the dynamic pressure (perturbation term) of the gland and the phase angle between deflection and the pressure for forward and backward precession, respectively. From these figures it is known that the dynamic pressure of the both cases is increased in proportion to the increase of rotating speed but that the tendency of the phase angle of both cases is the reverse.

MOTION PICTURE SUPPLEMENT

The 8-mm film was taken in order to observe the flow pattern in the gland of the labyrinth seal, where a continuous vortex in circumferential direction occurs. The vortex form is like a sinusoidal wave which is rotating in the same direction as the rotor. Figure 11 shows the two different flow patterns. The left side shows a conventional mathematical model of the flow pattern in the gland. This model is usually used to derive the fundamental equation. The real flow pattern is not similar to the model. In the gland the flow is composed of vortex and expansion flow as shown by the right side of figure 11.

Thus the next subject we should approach is the mathematical derivation of the fundamental equation considering the vortex in the gland.

CONCLUSIONS

The force induced by the labyrinth seal is solved by using the finite difference method, expressed in proportional terms to the velocity and displacement of the rotor, and reduced to the expression of oil-film force of journal bearings. Then the effect of the coefficients of the induced force on the stability of the rotor system is discussed from the energy point of view. The force induced by the labyrinth seal always makes the rotor system unstable, and the tendency is remarkable when leakage of the seal is small. The flow pattern in the labyrinth seal was investigated experimentally, and it is known that a continuous vortex in the circumferential direction occurs in the fluid flow. The form is like a sinusoidal wave which is rotating in the same direction as the rotor.

EDITORIAL SUPPLEMENT

Reproduction of the film frame (fig. 8) was not very successful, so we introduce figures 12 and 13 in an attempt to demonstrate the film supplement. Figure 12 is a sketch of what appears in the film to be a spiral vortex. Figure 13 represents a possible sequence of motions of the vortex center resulting from the periodic behavior of the flow interface. One must also be aware of the possible disturbance caused by the air bubbles in the flow field.

These instabilities appear to be linked with those noted in unpublished work by Robert C. Hendricks and T. Trent Stetz of the NASA Lewis Research Center, where a flow visualization study was carried out on a water table to determine some characteristics of flows through sequential Borda-type inlets (no rotation and no centerbody). In figure 14(a) the four lucite Borda models were placed in such a way that they touched each other to form a continuous channel. The inlet water depth was similar to the passage width. The injected dye revealed that the flow through this configuration continued uninterrupted after passing the vena-contracta. The models were then placed with spacings of 1/3 of the channel passage width (fig. 14(b)). The flow still continued in an uninterrupted manner after the vena-contracta. The models were then placed with spacings of 3/2 of the channel passage (fig. 14(c)). At this separation distance part of the flow entered the cavities and slight oscillations were observed. At a separation distance of 2-1/4 channel passage widths a very strong oscillation was observed (fig. 14(d)): The exhaust of one passage would "fan" the flow across the inlet of the subsequent Borda passage. These oscillations weakened when the separation distance was increased to 4 channel passage widths (fig. 14(e)). A separation of 6 channel widths showed minor oscillations (fig. 14(f)). At distances beyond 16 channel widths the flow through each Borda passage appeared nearly independent of the preceding flow (fig. 14(g)).

REFERENCES

(1) Kostyuk, A. G.: A Theoretical Analysis of the Aerodynamic Forces in the Labyrinth Glands of Turbomachines. Teploenergetica, 1972, vol. 19, no. 11, pp. 29-33.

(2) Kostyuk, A. G.: Circulation Forces over the Shrouding and Their Influence on the Threshold Capacity of Large Turbine Unit." Teploenergetica, 1975, vol. 22, no. 3, pp. 41-46.

BIBLIOGRAPHY

Alford, J. S.: Protecting Turbomachinery from Self-Excited Rotor Whirl. Trans. ASME, J. Eng. Power, Oct. 1965, pp. 333-344.

Spurk, J. K. and Keiper, R.: Selbsterregte Schwingungen bei Turbomachinen infolge der Labyrinthströmung. Ingenieur-Archiv, vol. 43, 1974, pp. 127-135.

Thomas, H. J.: Zur Laufstabilität einfacher Turborotoren, besonders bei Spalterregung. Konstruktion, vol. 30, 1978, H.9, pp. 339-344.

Wright, D. V.: Air Model Tests of Labyrinth Seal Forces on a Whirling Rotor. Trans. ASME, J. Eng. Power, Oct. 1978, pp. 533-543.

TABLE 1. - CALCULATION MODELS OF LABYRINTH SEAL FORCE

MODEL	Rs(mm)	l(mm)	θ(rad)	δ(mm)	WHIRL DIREC.	WHIRL FREQ.
A	40	10	0	0.3	FORWARD	ω_n
B	40	10	0	0.45	FORWARD	ω_n
C	40	10	0	0.6	FORWARD	ω_n
D	40	10	0	0.3	FORWARD	$0.5\ \omega_n$
E	40	10	0	0.3	BACKWARD	ω_n
F	40	10	0	0.3	FORWARD	$2\ \omega_n$
G	40	10	0	0.2 0.3 0.4	FORWARD	ω_n
H	40	10	0	0.4 0.3 0.2	FORWARD	ω_n

TABLE 2. - DATA OF ROTOR

FOR CALCULATION

Rs	0.04	m
m	1.98	Kg
k	2503.6	Kg/m
ω_n	111.45	rad/sec

TABLE 3. - DATA OF GAS

FOR CALCULATION

T	573	K
R	29.23	Kg m/Kg K
α	0.7	
p_0	20000	Kg/m
p_z	10000	Kg/m

TABLE 4. - STEADY-STATE VALUES

MODEL	Q(Kg sec/m⁴)	P(1) (ata)	P(2) (ata)	P(3) (ata)	P(4) (ata)
A	0.5004×10^{-1}	2.0	1.7130	1.4377	1.0
B	$0.7592\cdot10^{-1}$	2.0	1.7049	1.4335	1.0
C	0.1019	2.0	1.7002	1.4394	1.0
D	$0.5004\cdot10^{-1}$	2.0	1.7130	1.4377	1.0
E	$0.5004\cdot10^{-1}$	2.0	1.7130	1.4377	1.0
F	$0.5004\cdot10^{-1}$	2.0	1.7130	1.4377	1.0
G	$0.4373\cdot10^{-1}$	2.0	1.3711	1.1621	1.0
H	$0.4375\cdot10^{-1}$	2.0	1.8546	1.6000	1.0

P(1): inlet pressure, P(2): first gland pressure

P(3): second gland pressure, P(4): outlet pressure

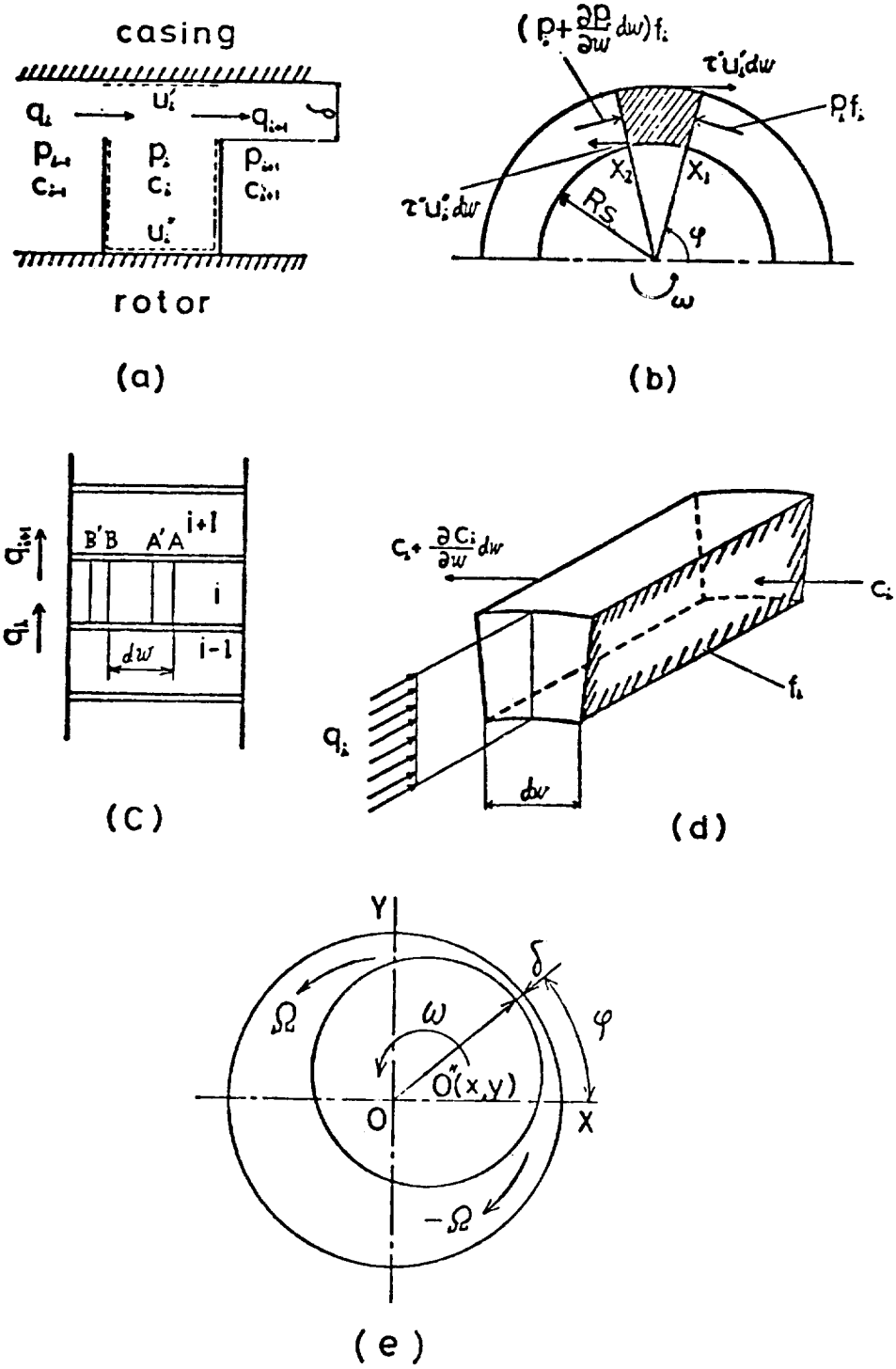

Figure 1. - Cross section of labyrinth seal and definition of coordinate.

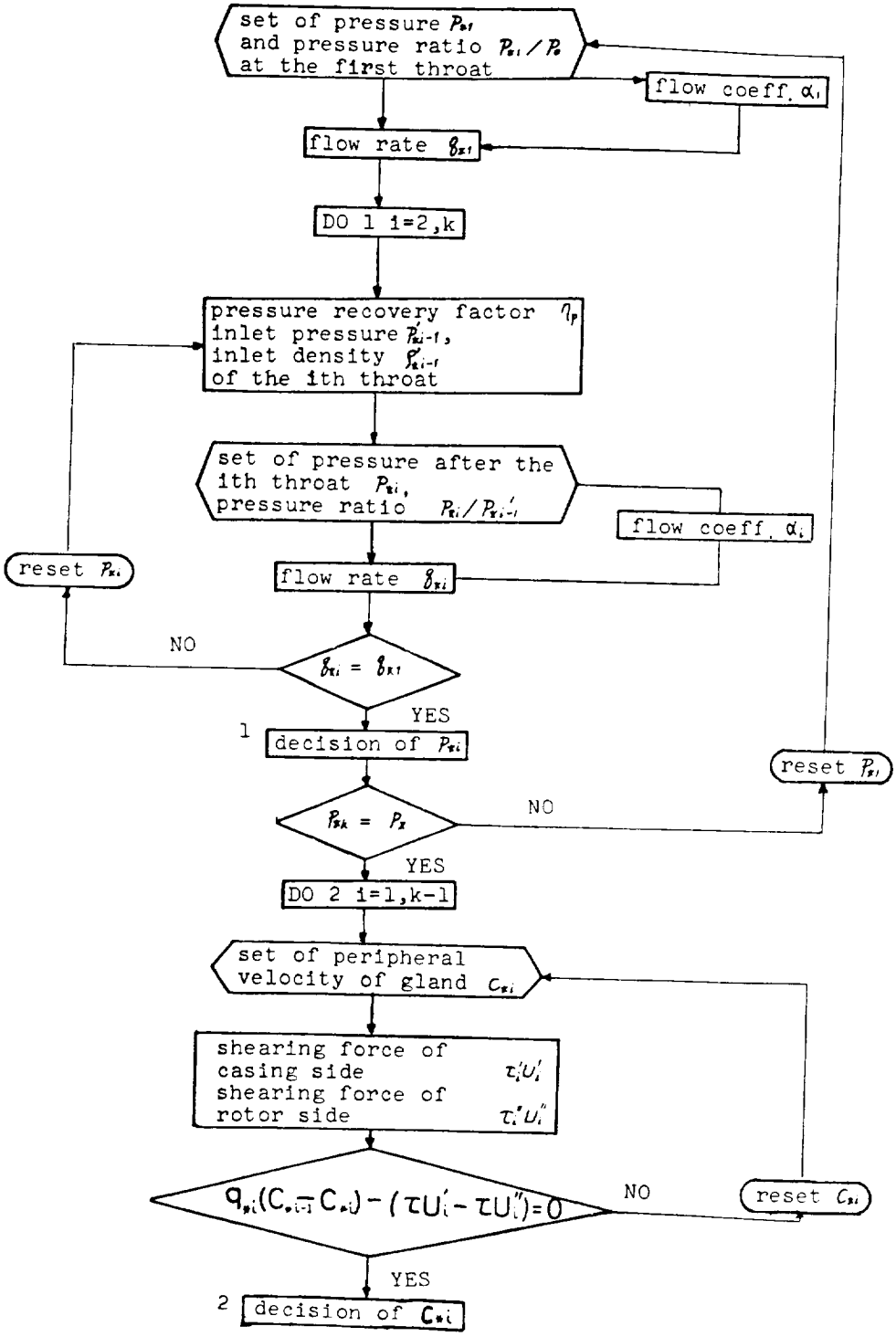

Figure 2. - Calculation procedure for steady state.

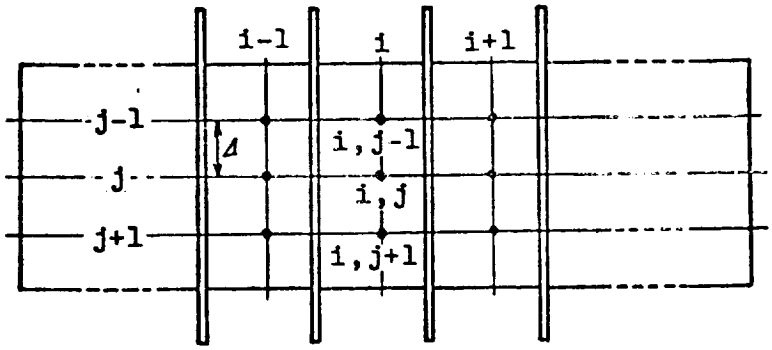

Figure 3. - Definition of mesh points for finite difference method.

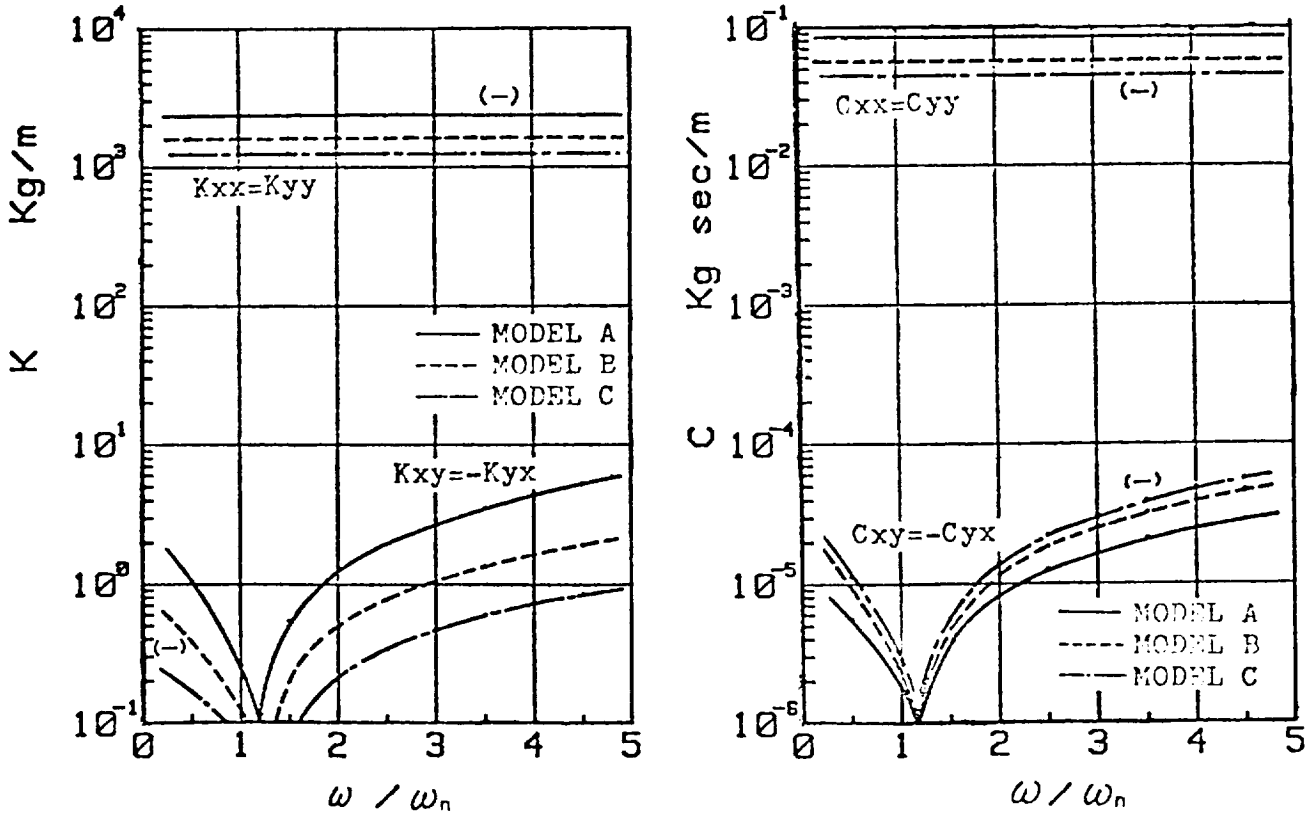

(a) Spring coefficients.

(b) Damping coefficients.

Figure 4. - Coefficients of flow-induced force for models A to C.

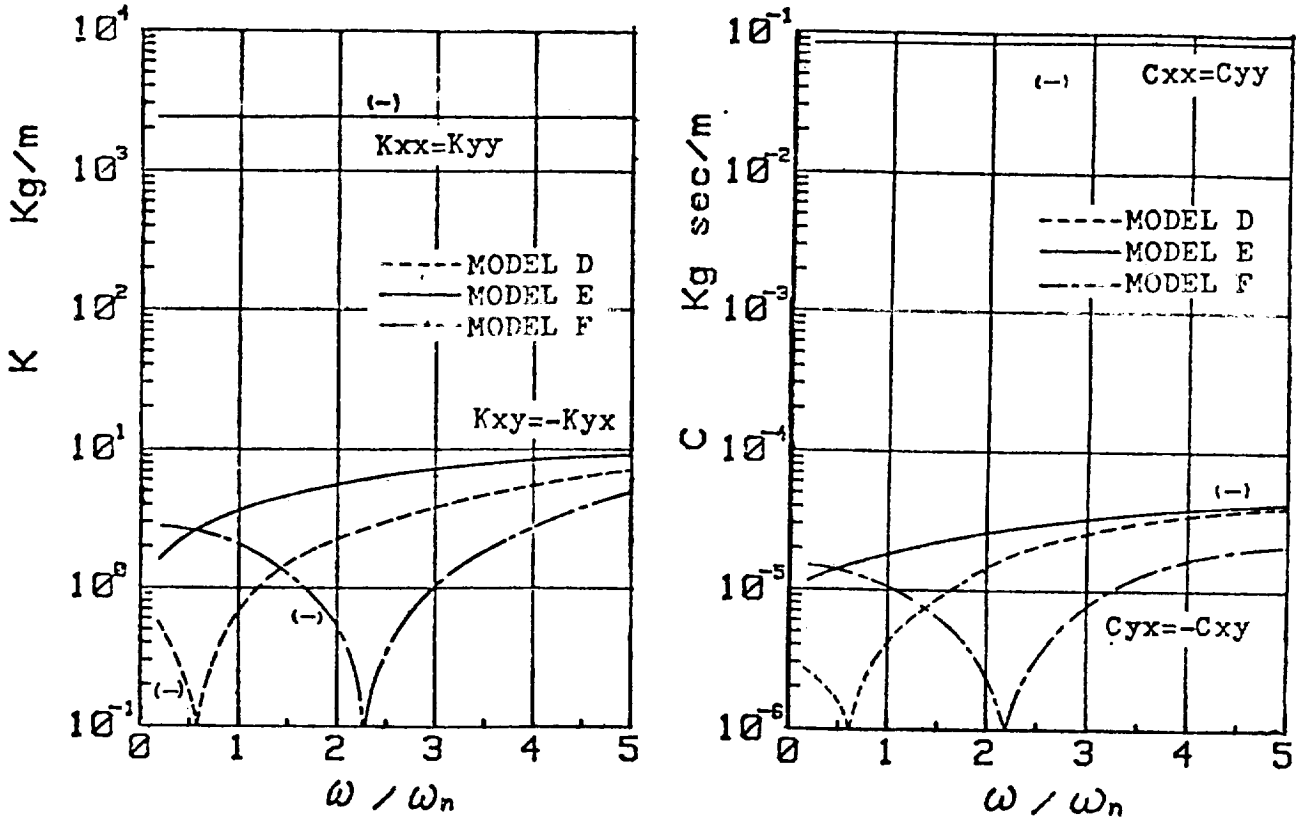

(a) Spring coefficients.

(b) Damping coefficients.

Figure 5. - Coefficients of flow-induced force for models D to F.

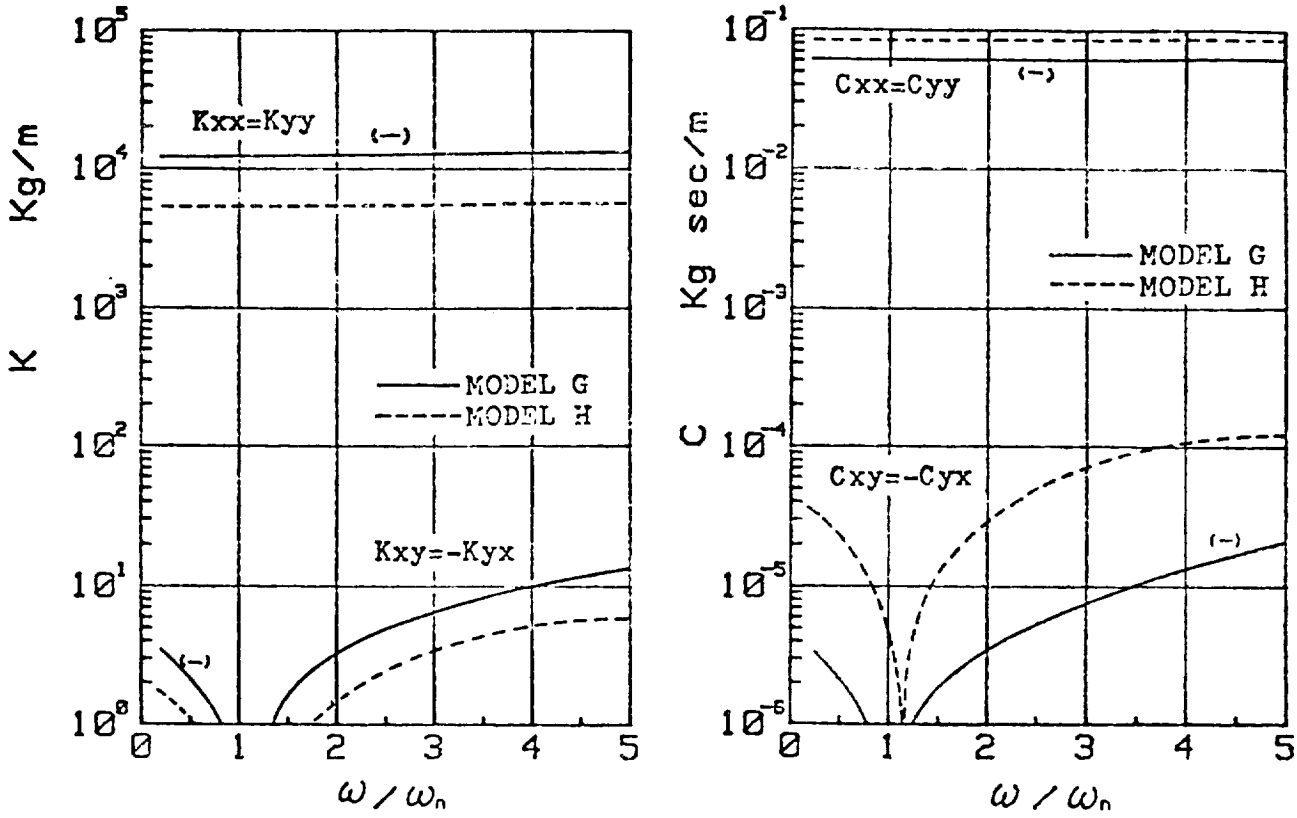

(a) Spring coefficients.

(b) Damping coefficients.

Figure 6. - Coefficients of flow-induced force for models G and H.

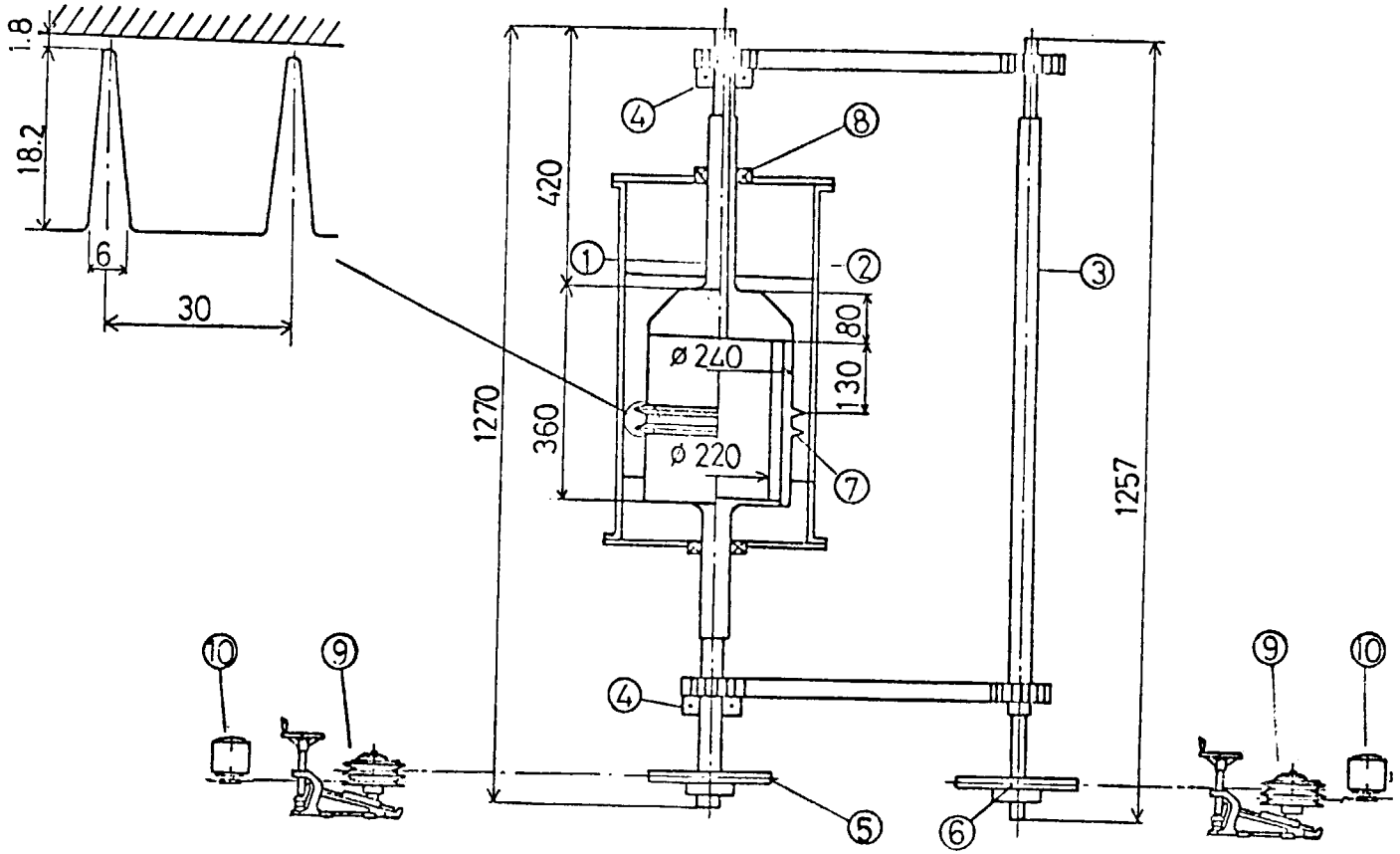

Figure 7. - Testing facility for labyrinth.

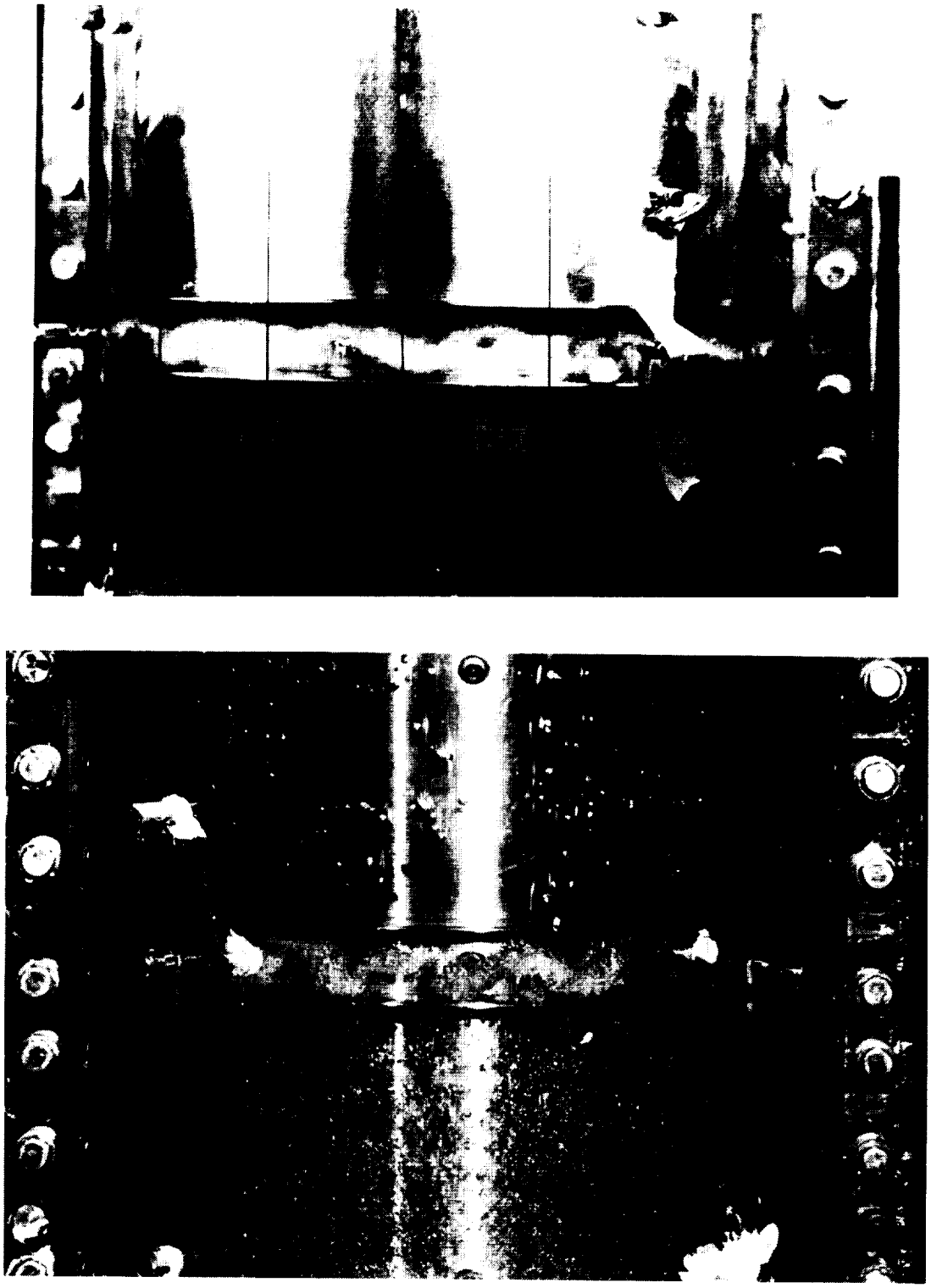

Figure 8. - Flow pattern in gland.

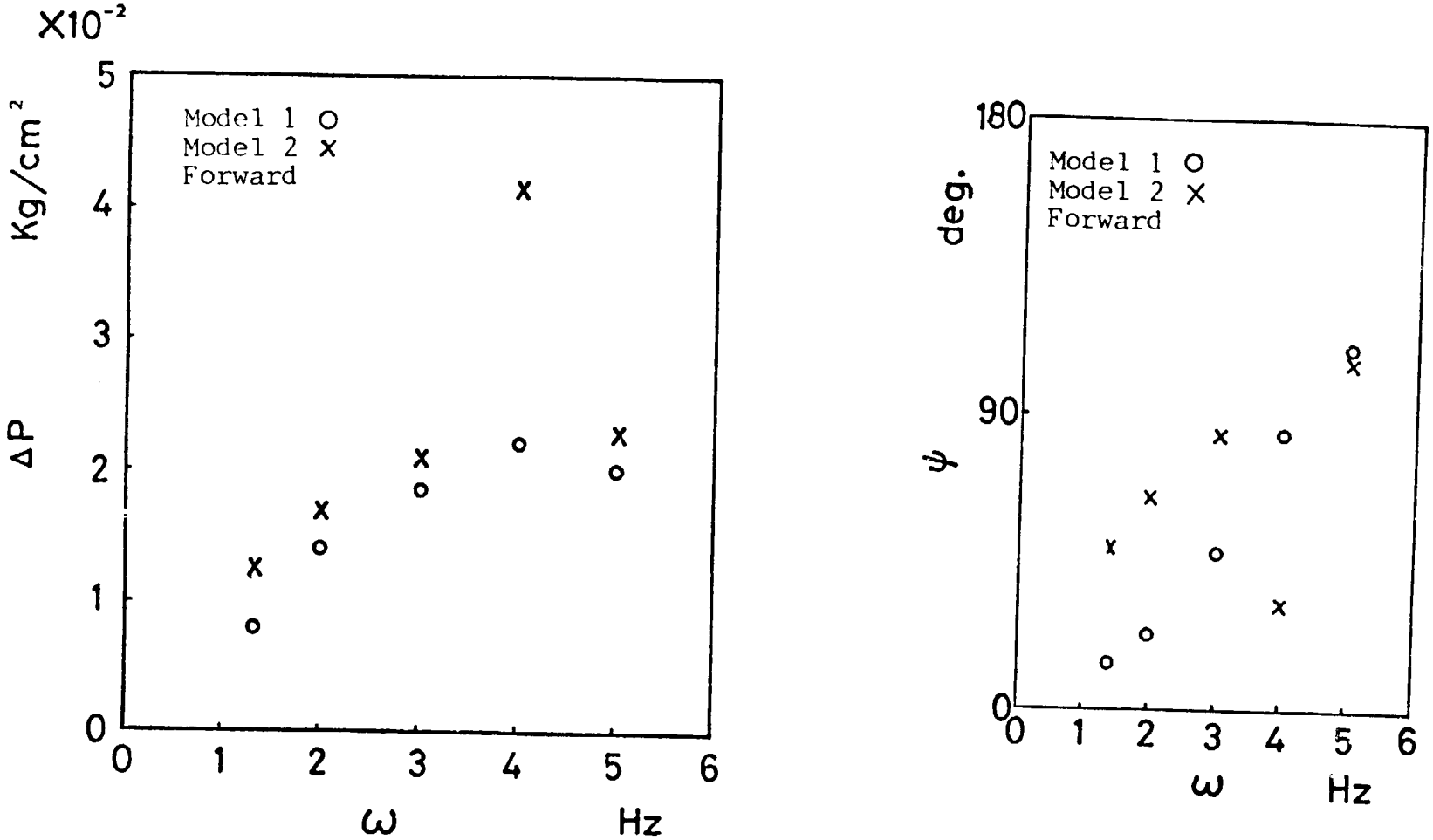

Figure 9. - Experimental results for forward precession.

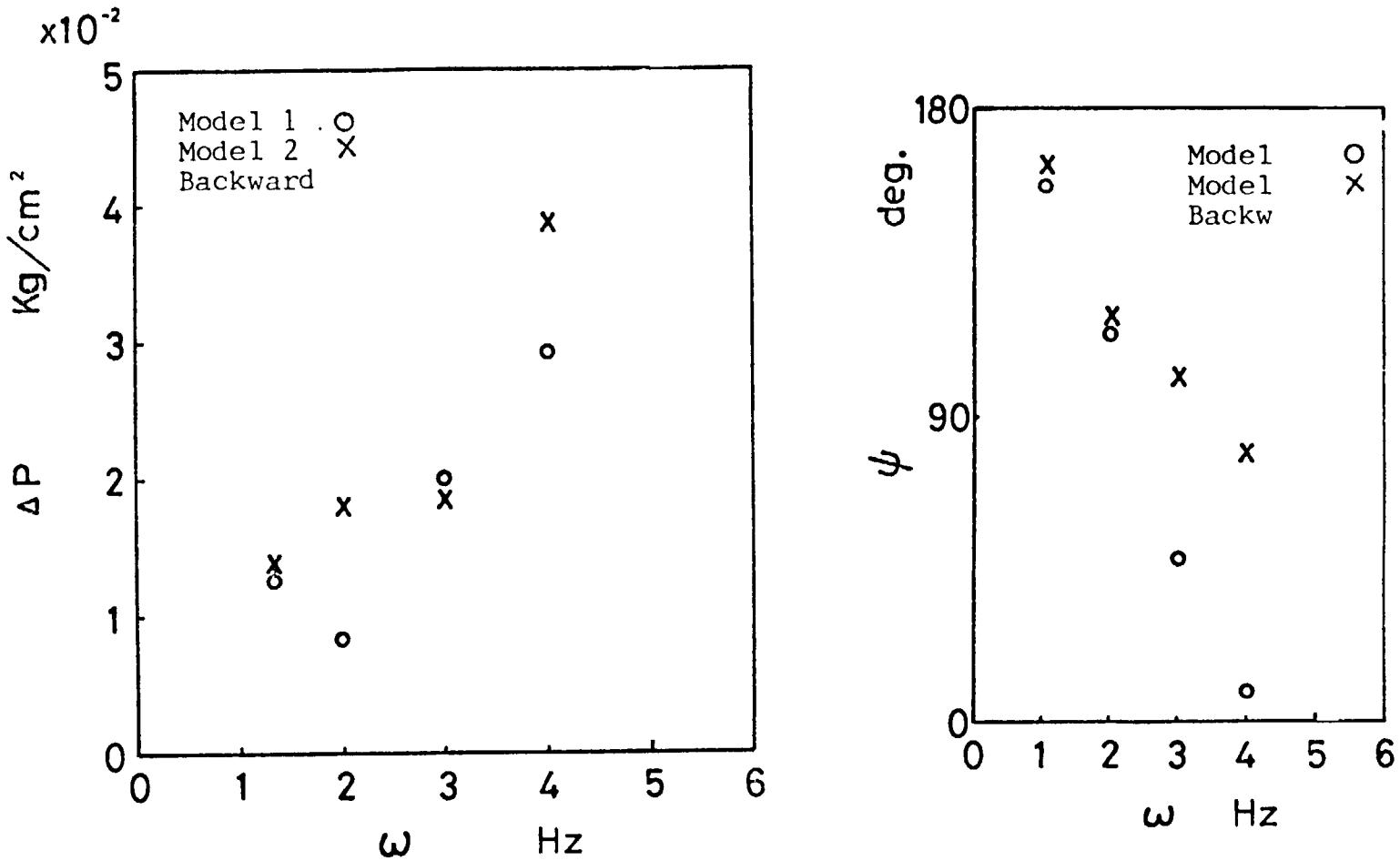

Figure 10. - Experimental results for backward precession.

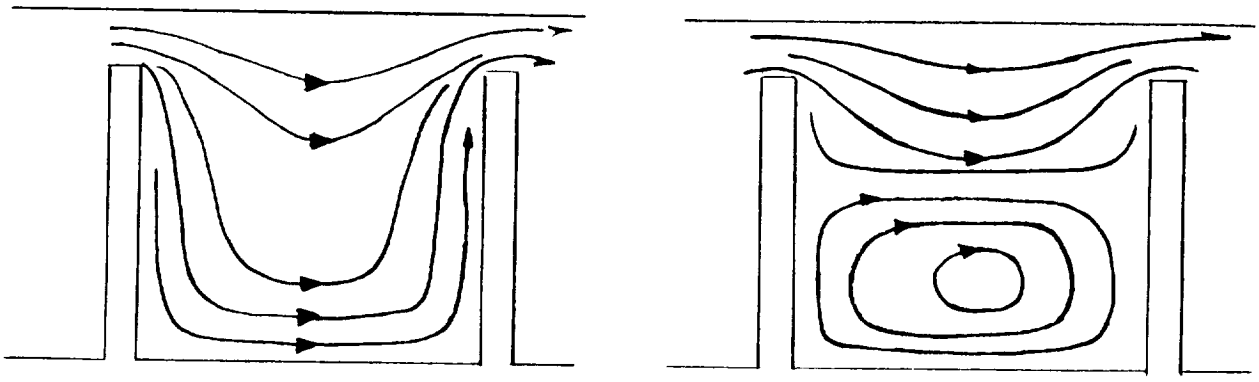

Conventional mathematical model

Real flow pattern

Figure 11. - Sketch of flow patterns.

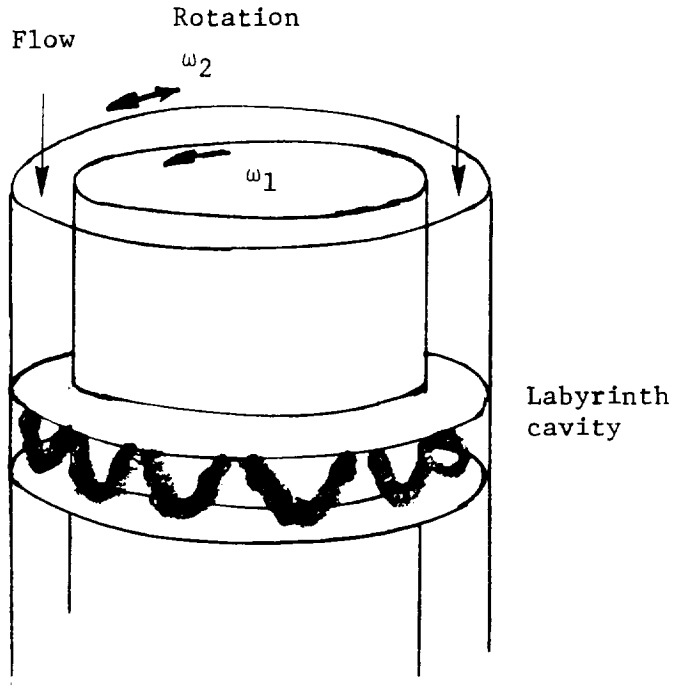

Figure 12. - Spiral vortex.

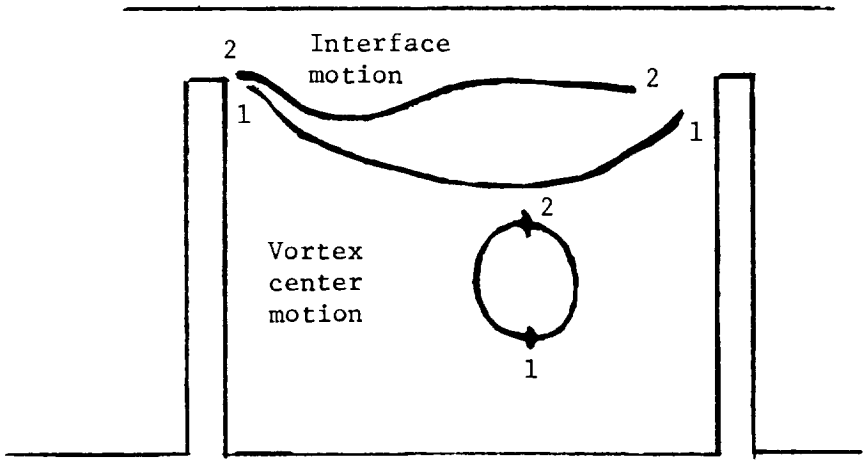

Figure 13. - Possible interface and vortex motions leading to a "spiral vortex."

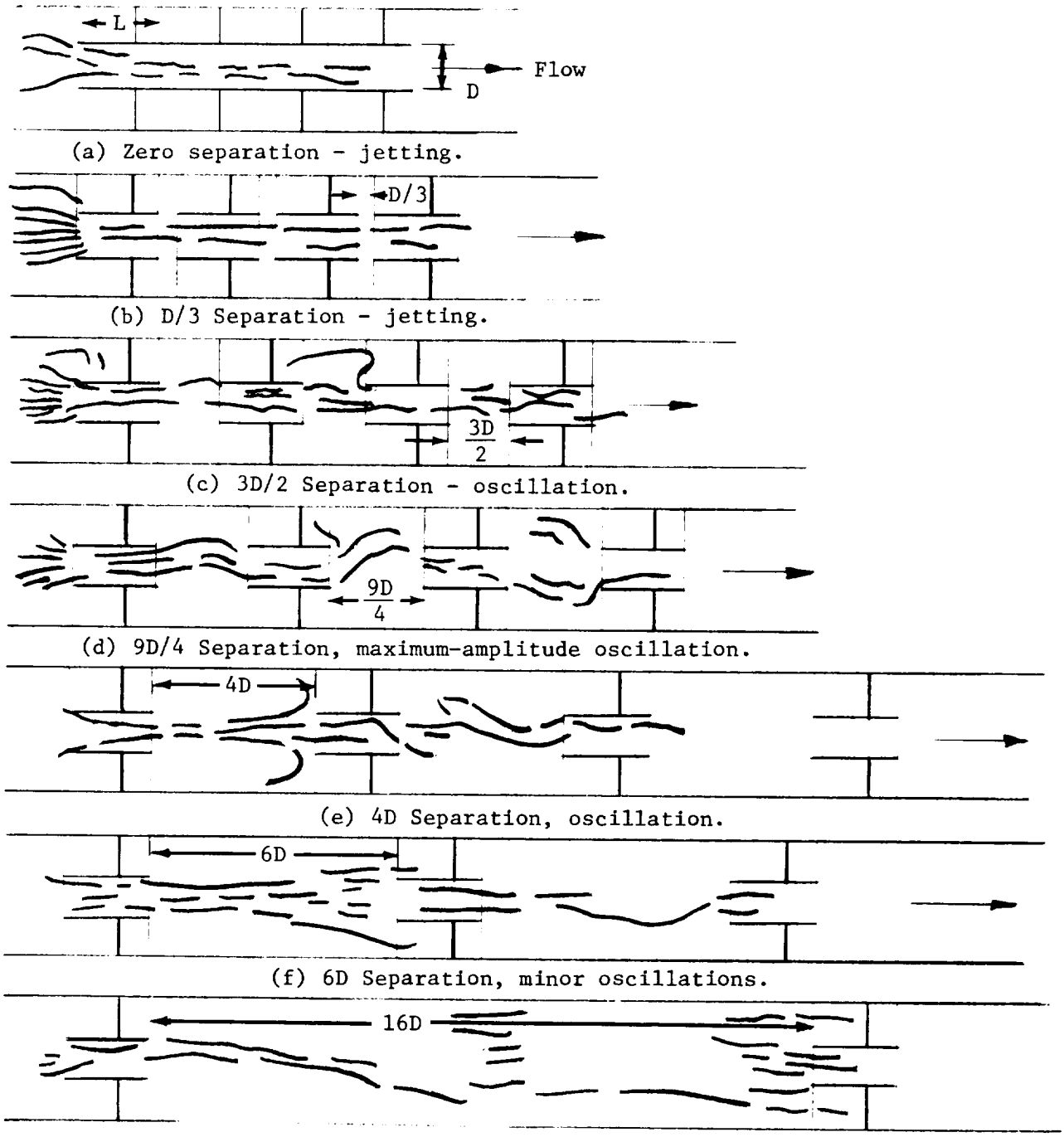

(a) Zero separation - jetting.

(b) D/3 Separation - jetting.

(c) 3D/2 Separation - oscillation.

(d) 9D/4 Separation, maximum-amplitude oscillation.

(e) 4D Separation, oscillation.

(f) 6D Separation, minor oscillations.

(g) 16D Separation, nearly independent of reservoir.

Figure 14. - Flow visualization of four sequential Borda-type inlets.